How to cite: *Angew. Chem. Int. Ed.* **2025**, *64*, e202413701
doi.org/10.1002/anie.202413701

Gas Separation | Hot Paper

Oriented Titanium-MOF Membrane for Hydrogen Purification

Sixing Chen[+], Mohammad Wahiduzzaman[+], Taotao Ji, Yi Liu, Yang Li, Chen Wang, Yanwei Sun, Gaohong He, Guillaume Maurin, Sujing Wang,* and Yi Liu**

Abstract: Precise hydrogen sorting from purge gas (H_2/N_2) and coke gas (H_2/CH_4), commonly carried out by cryogenic distillation, still suffers from low separation efficiency, high energy consumption, and considerable capital cost. Though still in its infancy, membrane technology offers a potential to achieve more efficient hydrogen purification. In this study, an optimum separation of hydrogen towards both methane and nitrogen via a kinetically-driven mechanism is realized through preferred orientation control of a MOF membrane. Relying on the 0.3 nm-sized window aligned vertical to the substrate, *b*-oriented Ti-MOF membrane exhibits ultra-high hydrogen selectivity, surpassing the upper bound limit of separating H_2/N_2 and H_2/CH_4 gas pairs attained so far by inorganic membranes. This spectacular selectivity is combined with a high H_2 permeability owing to the synergistic effect of the 1 nm-sized MOF channel.

Introduction

Separation process accounts for 45–55 % of global industrial energy consumption.[1] Although thermally driven-separation processes such as distillation, absorption, adsorption and rectification have been proven to afford highly purified products, alternative pressure-driven membrane separation may save > 90 % energy consumption.[2] Polymers have been the most widely used membrane candidates; nevertheless, the plasticization/swelling effect upon long-term operation inevitably limits their performance and they undergo a trade-off between permeability and selectivity, called as Robeson's upper bound.[3] Molecular sieve inorganic and hybrid membranes with regular and permanent pore channels are solid alternatives to polymer membranes towards transcending the upper-bound limit.[7] Metal–organic frameworks (MOFs) constructed from metal ion/cluster nodes linked to functional organic ligands through coordination bonds, have shown a great promise for energy-efficient separation, owing to their unprecedented topology richness, tunable pore size/shape aperture, and highly versatile functionality.[11] So far, MOF membranes have shown superior performances in terms of olefin/paraffin (e.g., C_3H_6/C_3H_8),[17] isomer (n-/i-C_4H_{10}),[18] as well as N_2/CH_4 separations.[19] Nonetheless, their effective application for the separation of small-sized gas, e.g., purge gas (H_2/N_2) and coke gas (H_2/CH_4) addressing energy-efficient hydrogen purification, ammonia production and light hydrocarbon recovery, is still to be achieved. Nonetheless, very few MOF membranes have been tested for this highly challenging separation with performance in terms of selectivity and permeability far to be optimum.[20] This is due to the complexity of achieving a strict control of the size and shape of small pores (in particular ~0.3 nm) due to the inherent flexibility of the MOF framework. Breaking the trade-off between H_2/N_2 and H_2/CH_4 selectivity and H_2 permeability using any types of molecular sieve membranes is therefore one of the biggest challenges in the field of membranes for gas separation.

MIP-177-LT (MIP stands for Materials from Institute of Porous Materials of Paris, LT for Low Temperature), a three-dimensional open framework connecting $Ti_{12}O_{15}$ clusters with formate ions, and 3,3′,5,5′-tetracarboxydiphenylmethane (mdip) ligands,[22] possesses 0.3 nm-sized pore window along the *b*-axis and 1.1 nm-sized channel along the *c*-axis (Figure 1a). The pore window along the *b*-axis falls between the kinetic diameters of H_2 (0.29 nm) and other

[*] S. Chen,[+] T. Ji, Y. Liu, Y. Li, Dr. C. Wang, Dr. Y. Sun, Prof. G. He, Prof. Y. Liu
State Key Laboratory of Fine Chemicals, Frontiers Science Center for Smart Materials, School of Chemical Engineering
Dalian University of Technology
Dalian, 116024 (China)
E-mail: diligenliu@dlut.edu.cn

Dr. M. Wahiduzzaman,[+] Prof. G. Maurin
Institute Charles Gerhardt Montpellier
Université Montpellier
Montpellier, 34293 (France)
E-mail: guillaume.maurin1@umontpellier.fr

Prof. S. Wang
Hefei National Research Center for Physical Sciences at the Microscale, Suzhou Institute for Advanced Research, and Hefei National Laboratory, CAS Key Laboratory of Microscale Magnetic Resonance
University of Science and Technology of China
Hefei, 230026 (China)
E-mail: sjwang4@ustc.edu.cn

Prof. Y. Liu
Dalian Key Laboratory of Membrane Materials and Membrane Processes
Dalian University of Technology
Dalian, 116024 (China)

[+] These authors contributed equally to this work.

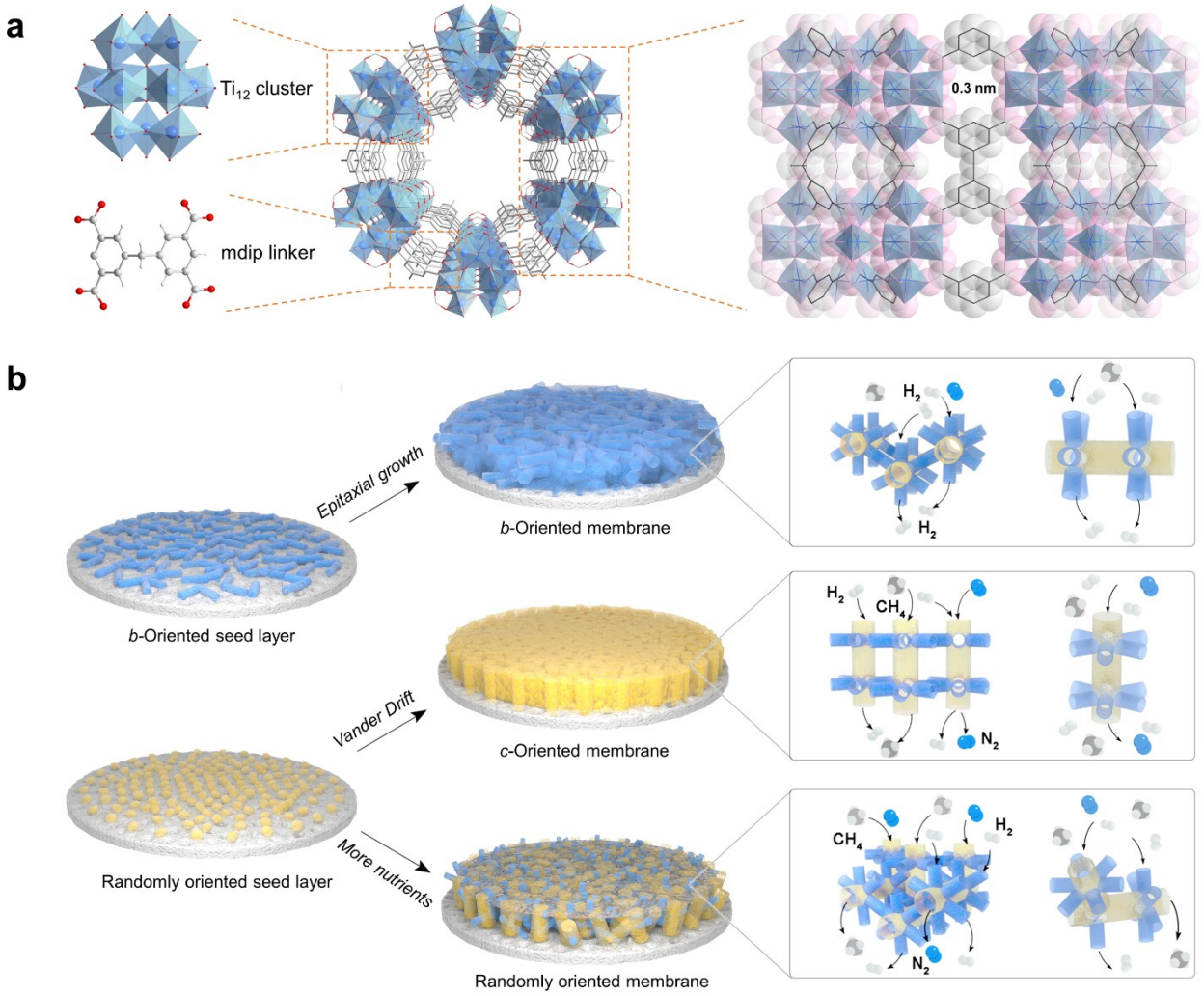

Figure 1. Crystal structure and schematic illustration of MIP-177-LT membranes. a) $Ti_{12}O_{15}$ cluster SBUs interlinked by H_4mdip linker and formate groups in the structure with views of the large hexagonal channel along the *c*-axis and the small pore windows along the *b*-axis. b) Fabrication of membranes with different possible preferred orientations and the envisioned gas diffusion pathways along the MOF pores.

larger gas molecules, e.g., N_2 and CH_4 with kinetic diameters of 0.36 nm and 0.38 nm respectively, offering a unique opportunity to achieve high H_2/N_2 and H_2/CH_4 selectivity via molecular-sieving and/or kinetically-driven processes. Moreover, the 1.1 nm-sized channel along the *c*-axis is expected to reduce the diffusion resistance, enabling to attain *a priori* high H_2 permeability. Nonetheless, irregular alignment of these channels may severely deteriorate the separation performance of this MOF.

Orientation control has been proven to be an effective strategy for uniform alignment of pore channels and elimination of grain boundary defects of MOF membranes, resulting in membranes with outstanding CO_2 capture performance.[25] Typically, Eddaoudi et al. prepared *c*-oriented mixed-matrix MOF membranes with unprecedented $CO_2/H_2S/CH_4$ separation performance through an ideal in-plan alignment of KAUST-8 nanosheets in polyamide matrix.[27] The benefit of fabricating highly orientated MOF membranes to boost their separation ability for other gas pairs, however, remains largely unexploited to date. As a proof-of-concept, with the objective to maximizing the hydrogen separation efficiency of such a membrane orientated via an epitaxial growth, we deliberately prepared *b*-oriented MIP-177-LT membrane (Figure 1b). Gas permeation tests demonstrated unprecedented selectivity for both H_2/N_2 (~150) and H_2/CH_4 (~120) coupled with H_2 permeability superior to 350 barrer, surpassing the upper bound limit of the conventional molecular sieve membranes reported so far for sorting these two highly challenging gas mixtures. This exceptionally high separation performance makes MIP-177-LT membrane as a great candidate for H_2 recovery from purge gas and coke gas under practical working conditions.

Results and Discussion

b-Oriented MIP-177-LT membrane was fabricated through oriented epitaxial growth. We revealed that the seed morphology, seed deposition condition, and epitaxial growth condition cooperatively contributed to the membrane formation. The first step involved the preparation of MIP-177-LT seeds. Uniform rod-shaped MIP-177-LT crystals with large aspect ratios were privileged since adopting such morphology was beneficial for vertical alignment of the 0.3 nm-sized pore windows. The aspect ratio of MIP-177-LT seeds was shown to be facilely tuned through adjusting chemical composition of the precursor solution with no effect on morphological uniformity (Figure S1). Through balancing preferred orientation and membrane continuity, MIP-177-LT crystals with aspect ratio of around 5.8 were selected as seeds (Figure S2). Thermogravimetric analysis (TGA) demonstrated that MIP-177-LT seeds are stable up to 280 °C, in line with the behavior of the bulk material (Figure S3).[22]

The next step referred to oriented deposition of MIP-177-LT seed layer. The proper seed suspension concentration to ensure uniform distribution of rod-shaped seeds on substrate and the introduction of surfactants to weaken their mutual interactions were identified as key parameters to control the fabrication of highly *b*-oriented MIP-177-LT seed layer. Trace amount of polyvinylpyrrolidone (PVP) containing several polar oxygen-containing groups was added to enhance the dispersion of MIP-177-LT seeds in suspension.[26] Indeed, we anticipated an enhancement of the MOF/polymer affinity by analogy with what has been previously reported for the preparation of highly (110)-oriented ZIF-7 seed layer.[28] We revealed that closely packed *b*-oriented MIP-177-LT seed layer can be obtained by spin-coating of the aqueous seed suspension containing trace amount of PVP, as magnified by SEM images (Figure 2a and Figure S4a).

It is also of utmost importance to prevent intergranular gaps and maintain preferred orientation inherited from the seed layer during epitaxial growth.[29] Well-intergrown MIP-177-LT membranes of 1.3 μm-thickness (Figure 2b-f) were thus prepared by optimizing the chemical composition of the precursor solution. The powder X-ray diffraction (PXRD) patterns of the resulting membranes (Figure S5a) only showed diffraction peaks at around 4.5° and 7.8°, assigned to (010) and (−120) planes, respectively, indicating the dominance of *b*-orientation.

For comparison, *c*-oriented MIP-177-LT membrane was equally fabricated through Van der Drift evolution principle,[30] widely adopted for orientation control of MOF membranes.[31] Since the growth rate of MIP-177-LT crystallites along the *c*-direction was much faster than that along other directions when seed crystals concatenate, crystallites growing closer to the *c*-direction would prevent further growth of the ones evolving along other directions. Eventually, *ab*-/*ac*- faces of MIP-177-LT crystallites tend to arrange in a direction perpendicular to the porous α-Al_2O_3 substrate, resulting in the formation of *c*-oriented MIP-177-LT membrane. The preparation of nano-sized MIP-177-LT seeds and precise control of the epitaxial growth kinetics of the MIP-177-LT seed layer were essential for maintaining the desired orientation. Initially, morphological control of MIP-177-LT seeds was achieved by simply reducing formic acid concentration, resulting in the formation of spherical nanocrystals or low-aspect-ratio nanorods (Figure S6). Phase purity of the so-obtained MIP-177-LT seeds was confirmed by the analysis of PXRD data (Figure S5b), FT-IR (Figure S7), TGA (Figure S3), and N_2 physisorption data (Figure S8). Subsequently, uniform MIP-177-LT seed layer of 620 nm-thickness (Figure 2g and Figure S4b) was deposited on porous α-Al_2O_3 substrate (Figure S9) by spin-coating. Subsequentially, epitaxial growth was carried out. SEM images revealed the formation of well-intergrown MIP-177-LT membrane of 1.1 μm-thickness comprising vertically aligned nanorods following van der Drift evolution principle (Figure 2h–l). In comparison with the seed layer, the corresponding PXRD pattern (Figure S5b) of the MIP-177-LT membrane showed evident (001) diffraction peak at around 7.2°, demonstrating preferred *c*-orientation of the so-obtained membrane.

We equally prepared randomly oriented MIP-177-LT membrane through tailoring epitaxial growth conditions. According to the Van der Drift evolution principle, when

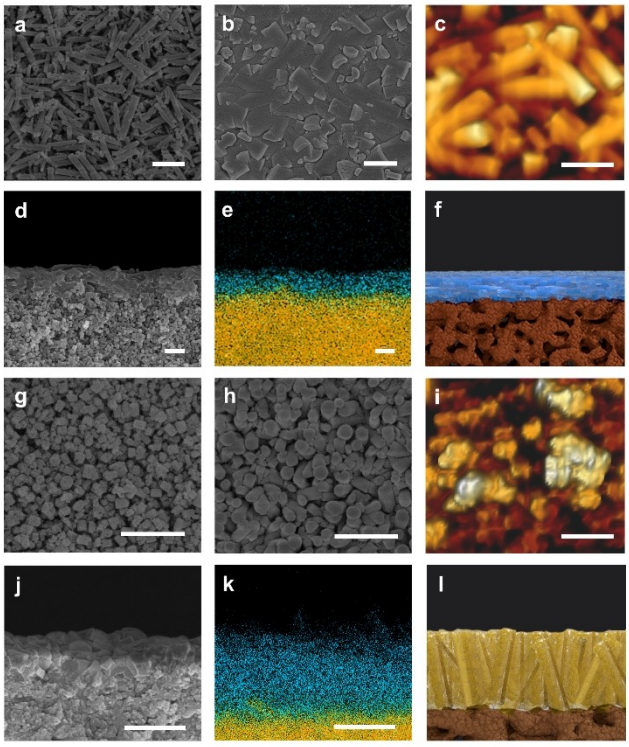

Figure 2. Morphology characterization of MIP-177-LT seed layers and membranes. a) SEM image of *b*-oriented MIP-177-LT seed layer. b-e) SEM, AFM and EDS images of *b*-oriented MIP-177-LT membranes. f) Schematic illustration of the cross-section of *b*-oriented MIP-177-LT membrane. g) SEM image of randomly oriented MIP-177-LT seed layer. h–k) SEM, AFM and EDS images of *c*-oriented MIP-177-LT membranes. l) Schematic illustration of the cross-section of *c*-oriented MIP-177-LT membrane. Scale bar: 1 μm.

the nutrient concentration of precursor solution is low, MIP-177-LT nanoparticles would evolve along the direction with the fastest growth rate, resulting in the formation of *c*-oriented membrane. In contrast, further increasing nutrient concentration would result in secondary nucleation in the bulk solution, followed by their random attachment to the substrate, thus ultimately leading to the formation of randomly oriented MIP-177-LT membranes. More specifically, the following factors were found to play decisive roles in fabrication of randomly oriented MIP-177-LT membrane: 1) The use of low-aspect-ratio MIP-177-LT nanocrystals as seeds; 2) surface modification of MIP-177-LT nanoseeds with PVP before spin-coating; 3) the employment of highly concentrated nutrients during secondary growth. SEM and EDS images (Figure S10a–c) show that well-intergrown MIP-177-LT membrane with 1.6 μm-thickness was obtained. The resulting PXRD pattern (Figure S10d) exhibited characteristic peaks at around 4.5°, 7.2°, 7.8°, 8.5° and 15.4° corresponding to (010), (001), (−120), (011) and (031) planes of MIP-177-LT, respectively, thus confirming random orientation of the resulting membrane.

Both single and mixed gas permeation tests were performed on *b*-oriented MIP-177-LT membrane at 120 °C and 1 bar of pressure corresponding to the condition commonly used to test membranes for the target gas mixtures separation. Single gas permeation measurements (Figure 3a) revealed that, H_2 permeability (351.0 barrer) is much higher than that for CO_2 (15.0 barrer), N_2 (2.6 barrer)

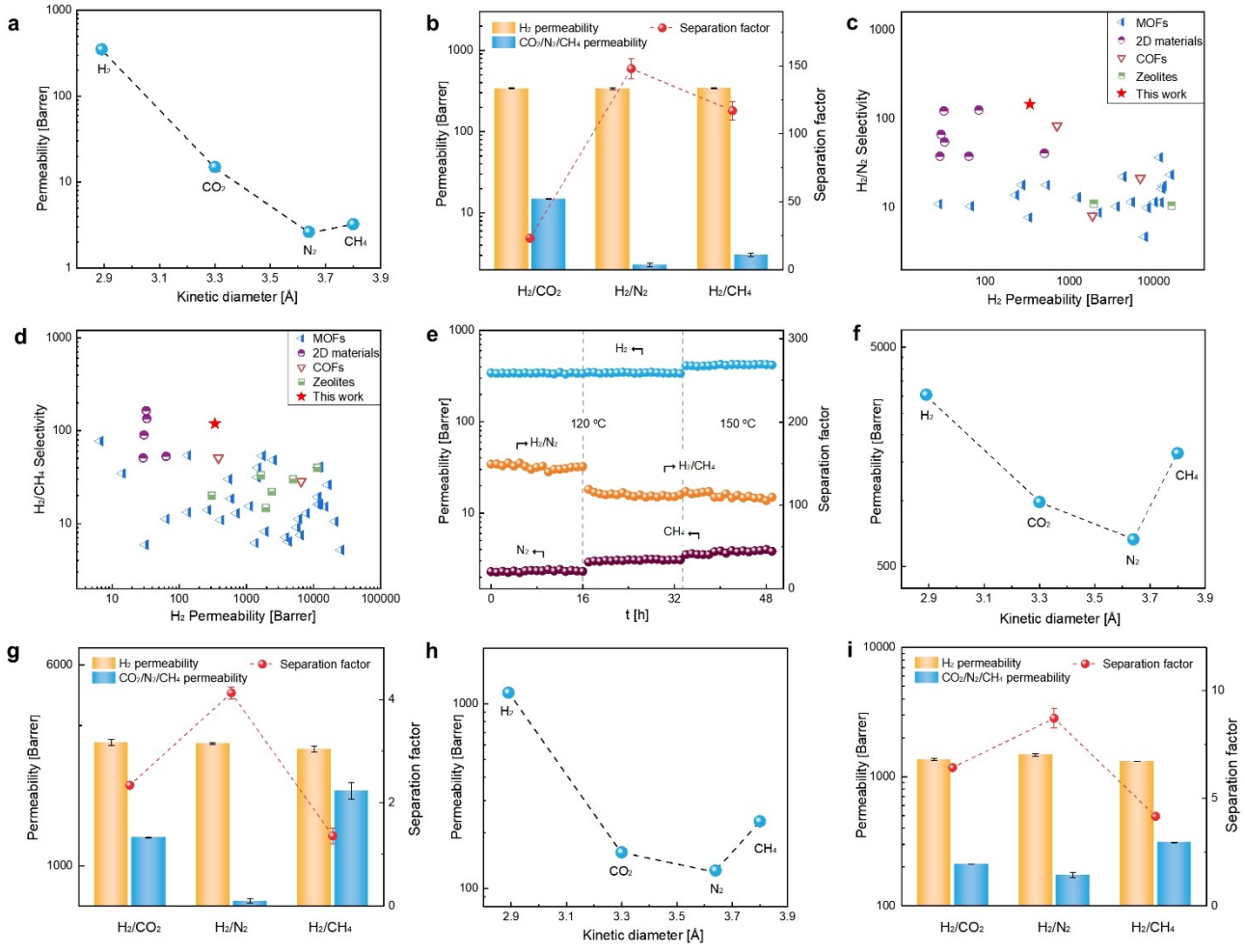

Figure 3. Separation performance of MIP-177-LT membranes. a) Single-gas permeation properties of *b*-oriented MIP-177-LT membrane. b) Equimolar mixed-gas separation performances of *b*-oriented MIP-177-LT membrane. Comparison of c) H_2/N_2 and d) H_2/CH_4 separation performance of *b*-oriented MIP-177-LT membrane at 120 °C and 1 bar of pressure with already reported membranes (the full list of membranes along with their references is provided in the Supporting Information as Table S1–4). e) Stability test of *b*-oriented MIP-177-LT membrane as a function of the operating temperature. f) Single-gas permeation properties of *c*-oriented MIP-177-LT membrane. g) Mixed-gas separation performances of *c*-oriented MIP-177-LT membrane. h) Single-gas permeation properties of randomly oriented MIP-177-LT membrane. i) Mixed-gas separation performances of randomly oriented MIP-177-LT membrane. Both single-gas permeation properties and mixed-gas separation performances of MIP-177 membranes with the three orientations were measured at 120 °C and 1 bar of pressure. Permeability and separation factor values are averaged over three samples, and error bars correspond to the standard deviation. Detailed data was listed in Table S8–S10.

and CH_4 (3.2 barrer). Moreover, separation factor (SF) of equimolar H_2/CO_2, H_2/N_2 and H_2/CH_4 gas mixtures reaches 23.1, 148.0 and 117.1 (Figure 3b), respectively. Atomistic insight into the H_2/CO_2, H_2/N_2, and H_2/CH_4 separation mechanisms was further delivered by periodic density functional theory (DFT) calculations. In the view of *b*-oriented MOF membrane, the gas diffusion pathway is expected to pass throughout a rectangular aperture-channel of the MOF with a dimension of about 0.3 nm. As such, diffusing gas molecules were predicted to effectively encounter two energy barriers at the entrance and exit of the aperture-channel prior to entering the large hexagonal channels. The calculated DFT minimum energy path (MEP) profiles for H_2, CO_2, N_2, and CH_4 passing through the small aperture-windows of MIP-177-LT (*b*-direction) led to diffusion energy barriers of ~20, ~35, ~60, and ~100 kJ/mol at the aperture windows, respectively (Figure 4). Note that for CO_2 a second energy barrier of ~24 kJ/mol arises from the middle of the aperture channel in addition to the effective barriers at the entrance/exit of the pore aperture resulting from strong coulombic repulsion between this molecule and the pore wall while aligning parallel to the aperture channel (Figure S11). Remarkably, the sequence of the predicted diffusion energy barriers through the small aperture channel of the MOF strongly suggests a faster transport of H_2 over CO_2, N_2 and CH_4 through the small-aperture windows of MIP-177-LT and indeed kinetically-driven separation mechanism for the *b*-oriented MIP-177-LT membrane. Notably, these simulations support the substantially higher permeability of H_2 observed experimentally for the *b*-oriented MIP-177-LT membrane as well as the much lower H_2/CO_2 selectivity than that for H_2/N_2 and H_2/CH_4 based on the energy barrier difference for the related gas pairs. Likewise, the DFT-derived host–guest interaction energy on the surface of the larger hexagonal channel – i.e., outside the restricting aperture channel – is much lower for H_2 (−8 kJ/mol) compared to the other gas molecules (CO_2: −26 kJ/mol, N_2: −17.5 kJ/mol and CH_4: −17 kJ/mol) that contributes to facilitate its migration towards the entrance of the MOF pore.

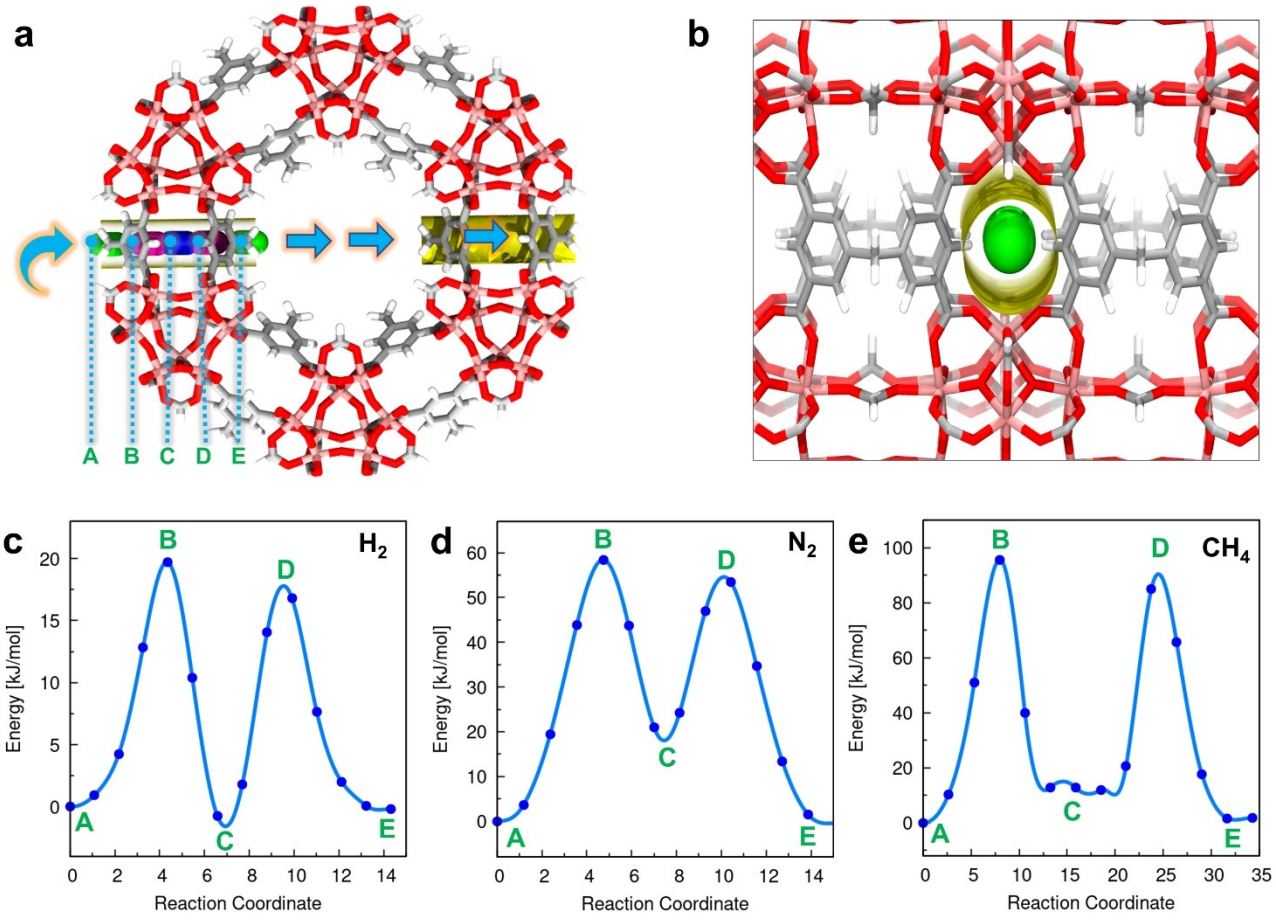

Figure 4. DFT-derived minimum energy pathways (MEPs) for the diffusion of the guest molecules through the small aperture of MIP-177-LT along the *b*-direction. a) Schematic representation of the diffusion pathway considered for the evaluation of the MEP for the transport of gas molecules. b) Microscopic view of a N_2 molecule passing thorough the small windows. c–e) MEPs for the diffusion of H_2, N_2 and CH_4, respectively. The five points A–E in Figure 4c–e correspond to the five positions in Figure 4a, respectively.

Decisively, the overall H_2/N_2 and H_2/CH_4 separation performance of *b*-oriented MIP-177-LT membrane spectacularly transcends the state-of-the-art Robeson upper bound plots, indicating the unique potential of this newly designed membrane for purge gas and coke gas purification (Figure 3c–d, Table S1 and Table S2). Of particular note, not only the H_2/N_2 selectivity (148.0) of our orientated Ti-membrane ranks the highest among molecular sieve membranes, but also the H_2 permeability (338.7 barrer) is one order of magnitude higher than the value exhibited by other highly H_2/N_2 selective membranes. Typically, the state-of-the-art 2D MOF membranes, e.g., $Zn_2(bIm)_4$ and MAMS-1, exhibit already 20 % lower H_2/N_2 selectivity (ca. ~120) while their H_2 permeabilities are extremely low, i.e. 4 times lower (< 85 barrer), due to the small pore size of this MOF (< 0.3 nm) and resultant gas tortuous diffusion path.[20] In sharp contrast, herein relying on the coupling effect between 0.3 nm-sized window and 1.1 nm-sized channel crossly aligned vertical to the substrate, the *b*-oriented MIP-177-LT membrane is highly H_2 selective without compromising gas permeability. In the same manner, the H_2/CH_4 separation performance (H_2 permeability: 342.2 barrer; H_2/CH_4 selectivity: 117.1) of this oriented membrane transcends other types of molecular sieve membranes (Figure 3d). Simultaneously, H_2/N_2 and H_2/CH_4 separation performances of *b*-oriented MIP-177-LT membrane can even rival the state-of-the-art MOF-based mixed-matrix membrane and polymer membrane (Figure S12, Table S1–S7), thereby demonstrating great promise for energy-efficient coke gas recovery.

Furthermore, we revealed that the separation factors for both equimolar H_2/N_2 and H_2/CH_4 gas mixtures through *b*-oriented MIP-177-LT membrane (95.6 and 56.2 respectively at 25 °C) steadily increases with increasing temperature reaching maximum values at 120 °C (148.0 and 117.1 respectively) and then decrease at 180 °C (100.1 and 94.5 respectively) (Figure S13 and Figure S14). It is well-known that gas permeability of polymer membranes increases with temperature at the expense of decreased selectivity. However, smaller pore-sized MOF membranes (such as MIP-177-LT) commonly exhibit superior separation performance at higher operation temperature due to the disappearing adsorption capacity of $CO_2/N_2/CH_4$ with increasing temperature.

Finally, operation stability of the membrane was investigated. We demonstrated that not only the H_2 permeability but also the separation factors for equimolar H_2/N_2 and H_2/CH_4 gas pairs remain constant within 50 h at 120 °C (Figure 3e), supporting that *b*-oriented MIP-177-LT membrane possesses excellent operation stability at optimum temperature of 120 °C. In addition, highly selective membranes commonly suffer from pressure-ratio limitations. Therefore, maintaining such selectivity at high pressure and with various stage cuts will be the scope of our future studies.

For comparison, gas permeation tests performed on *c*-oriented MIP-177-LT membrane revealed that the separation factor for the equimolar H_2/CO_2, H_2/N_2 and H_2/CH_4 gas pairs is very low and only reaches 2.3, 4.1 and 1.3 (Figure 3f–g), owing to vertical alignment of 1.1 nm-sized pore channel. A poor selective behavior was also observed for the randomly oriented MIP-177-LT membrane with separation factor for the equimolar H_2/CO_2, H_2/N_2 and H_2/CH_4 gas pairs of 6.4, 8.7 and 4.2 respectively (Figure 3h–i), which are much lower than the values achieved by the *b*-oriented MIP-177-LT membrane owing to concurrent exposure of 0.3 nm and 1.1 nm-sized pores to the gas flow. Decisively this comparison highlights that the fabrication of *b*-oriented MIP-177-LT membrane is optimum to favor straightforward pathways for the gases through the selective MOF pore to achieve an outstanding molecular discrimination. It should be noted that the Wicke-Kallenbach method has been widely employed in evaluating gas separation performances through measuring single gas and mixed gas permeation behaviors in molecular sieve membranes. Nevertheless, they might be overestimated because of the sweeping gas counterflow on the permeatie side.[32] Therefore, a cross-validation of experimental data using different measurement techniques,[33] such as constant volume method (which delivers a connection between the time lag, the adsorption equilibrium and diffusion parameters) and constant pressure method (which simulates industrial applications by continuous permeate composition), represents an important next step deserving future efforts.

Conclusions

Herein, we successfully fabricated MIP-177-LT MOF membranes with versatile preferred orientations. Aiming at H_2 purification, *b*-oriented membrane was conceived through preparing uniform length-to-width ratio rod-shaped seeds followed by controlled epitaxial growth. Owing to vertically aligned 0.3 nm-sized window, our membrane achieved ultra-high H_2/N_2 (148.0) and H_2/CH_4 selectivity (117.1) with overall separation performance surpassing state-of-the-art molecular sieve membranes. DFT simulations revealed that this superior selectivity comes from a strict control of the 0.3 nm-sized window aligned along the *b*-direction of the MOF that enables much easier passage of H_2 in comparison with N_2 and CH_4, confirming a kinetically-driven separation mechanism at the origin of the spectacular separation performance of the *b*-oriented membrane. In light of the advantage of membrane-based technology in terms of separation efficiency, energy consumption, and capital cost compared with traditional technologies, this newly designed membrane holds great promise for an effective H_2 separation from purge gas and coke gas.

Acknowledgements

The authors are grateful to Science Fund for Creative Research Groups of the National Natural Science Foundation of China (22021005, 22071234, 22078039, 22108025, 22205030), Fundamental Research Funds for the Central Universities (DUT22LAB602), National Key Research and Development Program of China (2019YFE0119200). M.W. and G.M. acknowledge GENCI-CINES for the HPC

resources to realize the computational work (Grant A0140907613).

Conflict of Interest

The authors declare no conflict of interest.

Data Availability Statement

The data that support the findings of this study are available from the corresponding author upon reasonable request.

Keywords: Gas Separation · Membranes · Metal–Organic Frameworks · Orientation · Rod-shaped crystals

[1] J. Y. S. Lin, *Science* **2016**, *353*, 121–122.
[2] D. S. Sholl, R. P. Lively, *Nature* **2016**, *532*, 435–437.
[3] L. M. Robeson, *J. Membr. Sci.* **2008**, *320*, 390–400.
[4] H. B. Park, J. Kamcev, L. M. Robeson, M. Elimelech, B. D. Freeman, *Science* **2017**, *356*, eaab0530.
[5] H. W. H. Lai, F. M. Benedetti, J. M. Ahn, A. M. Robinson, Y. Wang, I. Pinnau, Z. P. Smith, Y. Xia, *Science* **2022**, *375*, 1390–1392.
[6] M. R. Anderson, B. R. Mattes, H. Reiss, R. B. Kaner, *Science* **1991**, *252*, 1412–1415.
[7] Q. Song, S. Cao, R. H. Pritchard, B. Ghalei, S. A. Al-Muhtaseb, E. M. Terentjev, A. K. Cheetham, E. Sivaniah, *Nat. Commun.* **2014**, *5*, 4813.
[8] Z. Lai, G. Bonilla, I. Diaz, J. G. Nery, K. Sujaoti, M. A. Amat, E. Kokkoli, O. Terasaki, R. W. Thompson, M. Tsapatsis, D. G. Vlachos, *Science* **2003**, *300*, 456–460.
[9] J. Shen, Y. Cai, C. Zhang, W. Wei, C. Chen, L. Liu, K. Yang, Y. Ma, Y. Wang, C.-C. Tseng, J.-H. Fu, X. Dong, J. Li, X.-X. Zhang, L.-J. Li, J. Jiang, I. Pinnau, V. Tung, Y. Han, *Nat. Mater.* **2022**, *21*, 1183–1190.
[10] W. J. Koros, C. Zhang, *Nat. Mater.* **2017**, *16*, 289–297.
[11] H. C. Zhou, J. R. Long, O. M. Yaghi, *Chem. Rev.* **2012**, *112*, 673–674.
[12] Q. Qian, P. A. Asinger, M. J. Lee, G. Han, K. Mizrahi Rodriguez, S. Lin, F. M. Benedetti, A. X. Wu, W. S. Chi, Z. P. Smith, *Chem. Rev.* **2020**, *120*, 8161–8266.
[13] G. Liu, Y. Guo, C. Chen, Y. Lu, G. Chen, G. Liu, Y. Han, W. Jin, N. Xu, *Nat. Mater.* **2023**, *22*, 769–776.
[14] A. Knebel, A. Bavykina, S. J. Datta, L. Sundermann, L. Garzon-Tovar, Y. Lebedev, S. Durini, R. Ahmad, S. M. Kozlov, G. Shterk, M. Karunakaran, I. D. Carja, D. Simic, I. Weilert, M. Klüppel, U. Giese, L. Cavallo, M. Rueping, M. Eddaoudi, J. Caro, J. Gascon, *Nat. Mater.* **2020**, *19*, 1346–1353.
[15] G. Liu, V. Chernikova, Y. Liu, K. Zhang, Y. Belmabkhout, O. Shekhah, C. Zhang, S. Yi, M. Eddaoudi, W. J. Koros, *Nat. Mater.* **2018**, *17*, 283–289.
[16] T. Rodenas, I. Luz, G. Prieto, B. Seoane, H. Miro, A. Corma, F. Kapteijn, F. X. Llabrés i Xamena, J. Gascon, *Nat. Mater.* **2015**, *14*, 48–55.
[17] Y. Pan, T. Li, G. Lestari, Z. Lai, *J. Membr. Sci.* **2012**, *390–391*, 93–98.
[18] S. Zhou, O. Shekhah, J. Jia, J. Czaban-Jóźwiak, P. M. Bhatt, A. Ramírez, J. Gascon, M. Eddaoudi, *Nat. Energy* **2021**, *6*, 882–891.
[19] S. Zhou, O. Shekhah, A. Ramírez, P. Lyu, E. Abou-Hamad, J. Jia, J. Li, P. M. Bhatt, Z. Huang, H. Jiang, T. Jin, G. Maurin, J. Gascon, M. Eddaoudi, *Nature* **2022**, *606*, 706–712.
[20] Y. Peng, Y. Li, Y. Ban, W. Yang, *Angew. Chem. Int. Ed.* **2017**, *56*, 9757–9761.
[21] X. Wang, C. Chi, K. Zhang, Y. Qian, K. M. Gupta, Z. Kang, J. Jiang, D. Zhao, *Nat. Commun.* **2017**, *8*, 14460.
[22] S. Wang, T. Kitao, N. Guillou, M. Wahiduzzaman, C. Martineau-Corcos, F. Nouar, A. Tissot, L. Binet, N. Ramsahye, S. Devautour-Vinot, S. Kitagawa, S. Seki, Y. Tsutsui, V. Briois, N. Steunou, G. Maurin, T. Uemura, C. Serre, *Nat. Commun.* **2018**, *9*, 1660.
[23] M. Wahiduzzaman, S. J. Wang, J. Schnee, A. Vimont, V. Ortiz, P. G. Yot, R. Retoux, M. Daturi, J. S. Lee, J. S. Chang, C. Serre, G. Maurin, S. Devautour-Vinot, *ACS Sustainable Chem. Eng.* **2019**, *7*, 5776–5783.
[24] R. V. Pinto, S. J. Wang, S. R. Tavares, J. Pires, F. Antunes, A. Vimont, G. Clet, M. Daturi, G. Maurin, C. Serre, M. L. Pinto, *Angew. Chem. Int. Ed.* **2020**, *59*, 5135–5143.
[25] Y. Sun, Y. Liu, J. Caro, X. Guo, C. Song, Y. Liu, *Angew. Chem. Int. Ed.* **2018**, *57*, 16088–16093.
[26] Y. Sun, C. Song, X. Guo, Y. Liu, *ACS Appl. Mater. Interfaces* **2020**, *12*, 4494–4500.
[27] S. J. Datta, A. Mayoral, N. Murthy Srivatsa Bettahalli, P. M. Bhatt, M. Karunakaran, I. D. Carja, D. Fan, P. Graziane M Mileo, R. Semino, G. Maurin, O. Terasaki, M. Eddaoudi, *Science* **2022**, *376*, 1080–1087.
[28] S. Chen, Y. Sun, S. Chen, Y. Gao, F. Wang, H. Li, Y. Liu, *Chem. Commun.* **2021**, *57*, 2128–2131.
[29] Y. Liu, W. Qiang, T. Ji, M. Zhang, M. Li, J. Lu, Y. Liu, *Sci. Adv.* **2020**, *6*, eaay5993.
[30] A. Vanderdrift, *Philips Res. Rep.* **1967**, *22*, 267–288.
[31] Y. S. Li, H. Bux, A. Feldhoff, G.-L. Li, W.-S. Yang, J. Caro, *Adv. Mater.* **2010**, *22*, 3322–3326.
[32] T. H. Lee, Z. P. Smith, *Nat. Mater.* **2024**, *23*, 11–12.
[33] B. A. Al-Maythalony, O. Shekhah, R. Swaidan, Y. Belmabkhout, I. Pinnau, M. Eddaoudi, *J. Am. Chem. Soc.* **2015**, *137*, 1754–1757.

Manuscript received: July 20, 2024
Accepted manuscript online: September 24, 2024
Version of record online: November 6, 2024